Highly conductive ultrathin Co films by high-power impulse magnetron sputtering

L. Jablonka,[1] L. Riekehr, [1] Z. Zhang, [1] S.-L. Zhang,[1] T. Kubart,[1,a)]

[1]*Solid State Electronics, The Ångström Laboratory, Uppsala University, SE-75121 Uppsala, Sweden*

Ultrathin Co films deposited on SiO_2 with conductivities exceeding that of Cu are demonstrated. Ionized deposition implemented by high-power impulse magnetron sputtering (HiPIMS) is shown to result in smooth films with large grains and low resistivities, namely 14 μΩ cm at a thickness of 40 nm, which is close to the bulk value of Co. Even at a thickness of only 6 nm a resistivity of 35 μΩ cm is obtained. The improved film quality is attributed to a higher nucleation density in the Co-ion dominated plasma in HiPIMS. In particular, the pulsed nature of the Co flux as well as shallow ion implantation of Co into SiO_2 can increase the nucleation density. Adatom diffusion is further enhanced in the ionized process resulting in a dense microstructure. These results are in contrast to Co deposited by conventional direct current magnetron sputtering where the conductivity is reduced due to smaller grains, voids, rougher interfaces, and Ar incorporation. The resistivity of the HiPIMS films is shown to be in accordance with models by Mayadas-Shatzkes and Sondheimer that consider grain-boundary and surface-scattering.

[a]tomas.kubart@angstrom.uu.se

Cobalt is considered as a potential material for the metallization in future technology nodes with continued aggressive size downscaling.[1–4] Even though the bulk resistivity of Co (6.2 μΩ cm) is higher than that of Cu (1.678 μΩ cm), at such reduced dimensions the conductivity is mostly limited by surface scattering and the shorter electron mean free path in Co is beneficial.[1] Therefore, the conductivity of Co is predicted to be superior to Cu for linewidths smaller than 15 nm.[2] Furthermore, the much higher melting point of Co (1495 °C) compared to Cu (1084 °C) makes it more stable in terms of lower diffusivity and higher resistance to electromigration. For this reason, Co has already been considered as a liner material for Cu metallization.[5] In order to have room for the interconnect metal in extremely scaled interconnects liners need to be either ultrathin or even omitted entirely. Because of its superior stability, Co is a promising material candidate even for a liner free metallization process.

In order to achieve a satisfactory conductivity of Co, a deposition technique is required that yields Co films with high uniformity, smooth surfaces, large grains and low level of impurities. Although chemical vapor deposition and atomic layer deposition are the techniques of choice for ultrathin films with excellent coverage, the search for precursors that allow low growth temperatures, low level of contaminations, and nucleation on SiO_2 is still the subject of ongoing research.[6–8] Magnetron sputtering, a physical vapor deposition (PVD) technique, on the other hand, provides high purity materials and is used for metallization or seed layer deposition, but suffers from limited conformity. Some of the limitations of standard magnetron sputtering are eliminated by using ionized PVD where the deposition is carried out from ionized vapor.[9] The material ionization allows steering of the flux by electric fields, which can lead to an improvement of the conformity of the depositions and enhances the filling of narrow features by re-sputtering of the deposited material from the surface.[10] Classical ionized PVD techniques require complicated hardware where the vapor source is

complemented by a high density plasma ionization stage. To circumvent this complication, in high-power impulse magnetron sputtering (HiPIMS) a standard magnetron sputtering cathode is operated in a pulsed manner at a low duty cycle (typically below 1 %) and at a low frequency to achieve a very high peak power. Thus, peak power densities of about 1-10 kW/cm^2 are achieved, which is two orders of magnitude higher than in standard sputtering.[11] This leads to significantly enhanced ionization of the sputtered species with beneficial consequences for the properties of the deposited coatings such as increased density, enhanced adhesion, or improved microstructure.[12,13] Another advantage of the HiPIMS technique is its compatibility with standard magnetron sputtering hardware because the average discharge power is kept at values comparable to direct current magnetron sputtering (DCMS). Recently, HiPIMS deposition of Cu has been reported to lead to films with significantly reduced resistivity at thicknesses from 20 to 800 nm.[14]

In this paper, we study ionized PVD of thin and ultrathin Co films and focus on the nucleation of Co directly on SiO_2 at room temperature. We use HiPIMS and DCMS for the deposition and investigate the effects of ion energy and ion type on the electrical properties of the films. Compared to films deposited by standard DCMS, HiPIMS films have a better conductivity, which we attribute to beneficial growth conditions that result in bigger grains, higher density, and smoother surfaces.

All depositions were carried out in a Lesker CMS-18 ultra-high vacuum deposition system with a base pressure below 10^{-5} Pa. The system was equipped with four magnetron sputtering sources tilted with an angle of 16° in co-sputtering configuration. The target-to-substrate distance was approximately 180 mm. For the experiments, a single magnetron source Torus 2HV with a strong magnetic system assembly was used with a planar circular Co (99.95% purity) target with a thickness of 3 mm and a diameter of 50 mm. A 2 mm thick Cu spacer

was inserted between the magnetron body and the target to reduce the magnetic field strength on the target surface. The depositions were performed in Ar (99.9995 %) atmosphere at a constant pressure of 1.1 Pa and a mass flow of 80 sccm (standard cubic centimeter per minute). The substrates, thermally oxidized (100) Si with 250 nm of SiO_2, were placed on a rotating substrate holder and biased during the deposition. No intentional substrate heating was used. In both HiPIMS and DCMS the average discharge power was kept at 130 W. The HiPIMS sputtering power was delivered by a SIPP 1000 pulsing unit supplied by an Advanced Energy Pinnacle dc generator. Both the target current and voltage were monitored using current and voltage transducers, and recorded in an Agilent Infiniium (DSO9064A) digital oscilloscope, which was also used to calculate the instantaneous power delivered to the discharge and the average power. A pulse on-time of 50 μs and a frequency of 100 Hz were used and the average discharge power was kept at 130 W. The pulse power P_p is calculated from the energy per pulse as

$$P_p = \frac{\int_0^{T_{on}} I \times U \, dt}{T_{on}} \qquad (1)$$

where T_{on} is the pulse on-time. A unipolar bias with a pulse on-time of 120 μs was synchronized with the HiPIMS pulses. In DCMS the power was supplied by a Pinnacle Plus generator operated in continuous dc mode. The substrates were biased using bipolar pulsed dc bias (frequency of 50 kHz, 1.6 μs off time) in the DCMS experiments. For both deposition modes, bias values of -30 and -300 V were used initially. Complementary depositions were carried out at intermediate values of -100 and -200 V.

The sheet resistance of the Co films was measured using an Advanced Instrument Technology CMT-SR2000N four-point probe station with a tip diameter of 200 μm and a probe distance of 1 mm. The film thickness was controlled by the deposition time. Rutherford backscattering spectrometry (RBS) was used to calibrate the deposition rate and to identify Ar

incorporation into the Co films.. The surface morphology of the films was characterized by scanning electron microscopy (SEM) using a FE-SEM Zeiss Merlin equipped with an in-lens secondary electron detector and an energy selective backscattered electron detector. Cross-sectional TEM lamellas attached to a Cu lift-out grid were prepared with a FEI Strata DB235 dual beam focused ion beam / scanning electron microscope. The TEM micrographs were recorded with a FEI Titan Themis operated at an accelerating voltage of 200 kV. The film thickness measured by TEM was used to calculate the deposition rate. Grazing-incidence X-ray diffraction (GI-XRD) was performed with a Siemens D5000.

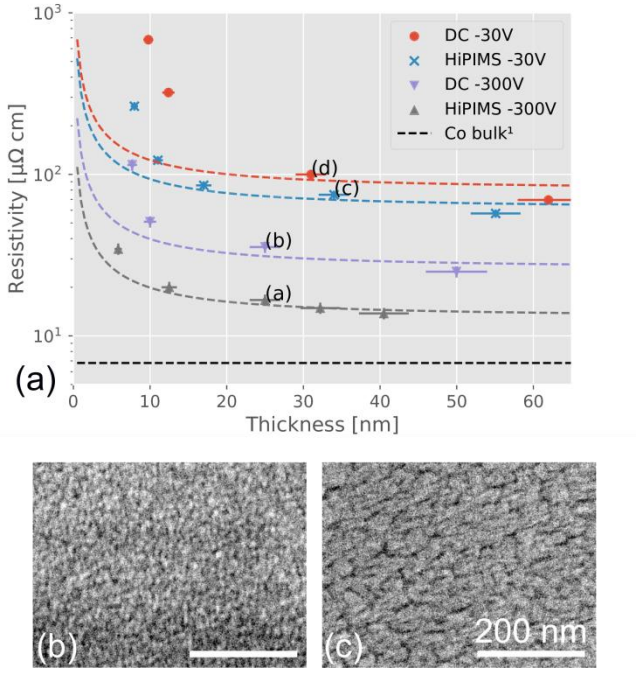

Figure 1 (a) Dependence of the Co film resistivity on the film thickness. The dashed lines show the calculated resistivity based on equations 3 and 5 as discussed in the text. The annotations (a-d) refer to samples characterized by TEM and shown in Figure 2 as well as discussed in Figure 3. The top-down SEM micrographs show (b) a HiPIMS -300 V film at 6 nm thickness and (c) a DCMS -30 V film at 12 nm.

The resistivity of the Co films as a function of film thickness is shown in Figure 1 for both deposition techniques and two values of ion energy (substrate bias). While the evolution of resistivity with thickness is similar for all four series, there is a huge difference in the absolute

values. The resistivities differ by nearly an order of magnitude and only the thickest, most conductive films have a resistivity close to the bulk resistivity[1] of Co of 6.8 μΩ cm. Since all the Co films are of the same hexagonal crystal structure (space group $P6_3/mmc$) as confirmed by GI-XRD, the difference in resistivity must arise from other structural properties. In the following text, we refer to the resistivities of the thicker films as "intrinsic" resistivities and discuss them in further detail based on TEM images, density calculations, and grain-boundary-scattering models. The increase in resistivity for thinner films, on the other hand, is usually attributed to the dominance of surface scattering and can be described by the Sondheimer model.[15] As shown later, the nucleation behavior has a considerable influence on the resistivity as well.

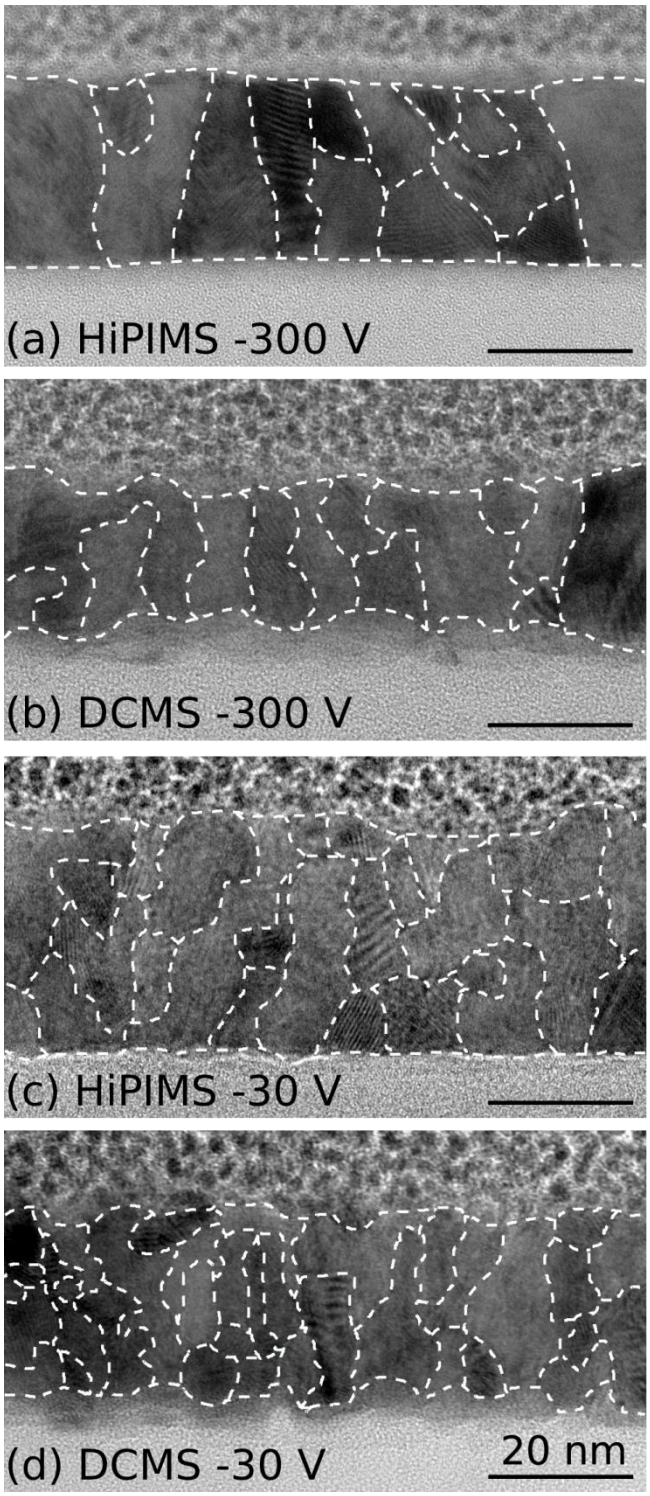

Figure 2 Cross-sectional TEM micrographs of Co films on SiO_2. (a) HiPIMS at -300 V, (b) DC at -300 V, (c) HiPIMS at -30 V, (d) DC -30 V. The dashed lines were added manually to highlight the grain sizes as estimated by the bright field contrast.

The resistivity is strongly dependent on the microstructure of the films. Cross-sectional TEM micrographs (Figure 2) give insight into the grain structure of the films. In particular,

the film with the lowest resistivity (HiPIMS, -300 V, Figure 2a) has grains that extend vertically through the film. In comparison, the film deposited by DCMS at the same substrate bias has smaller grains and a rougher SiO_2/Co-interface as well as a rougher Co surface (Figure 2b). At lower substrate biases (-30 V), the grain size is reduced further, especially in the vertical dimension, for both HiPIMS and DCMS (Figure 2c+d). While the interfaces of the HiPIMS film are smooth even at the lower ion energy (Figure 2c), the DCMS interfaces are rough in both cases (Figure 2b+d). Additional AFM measurements confirm that the root-mean-squared surface roughness of the -30 V DCMS film is increased compared to the -300 V HiPIMS film (0.94 nm vs. 0.21 nm, AFM scans not shown here). Some regions – mostly in films deposited at low ion energies – appear to be non-crystalline. From the TEM micrographs in Figure 2 alone it is however difficult to judge the crystallinity of such regions.

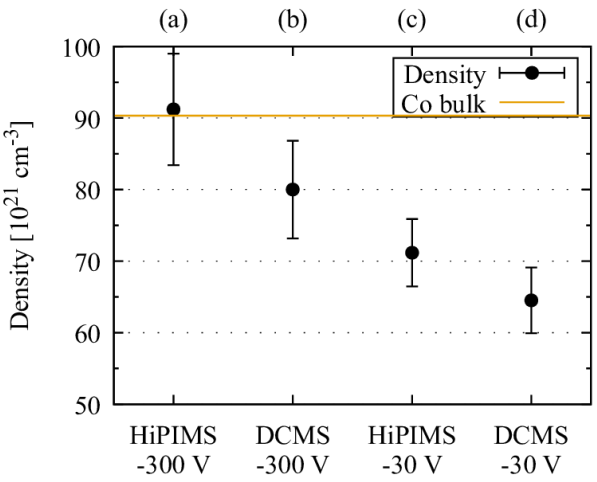

Figure 3 Atomic density of Co films. The labels (a-d) refer to the respective labels in Figures 1 and 2

The atomic density of the Co films is calculated from the TEM-measured film thickness and the RBS areal density (Figure 3). Although the sputtering rate was independent of the applied bias (HiPIMS: $0.06 \times 10^{15}\,\mathrm{at.\,cm^{-2}\,s^{-1}}$, DCMS: $0.25 \times 10^{15}\,\mathrm{at.\,cm^{-2}\,s^{-1}}$ as measured by RBS), the physical thickness and the density was strongly affected. While the density of the HiPIMS -300 V film is within range of the bulk value for hexagonal Co, the higher resistivity films exhibit a lower density. In the extreme case of DCMS -30 V, the

density is 30 % below the bulk value. Such low densities could be caused by the presence of voids or amorphous regions in the films (b-d), which, however, cannot be unambiguously identified from the contrast in the TEM images of Figure 2.

To model the resistivity in thick, polycrystalline films according to Mayadas and Shatzkes, the films are assumed to consist of columnar grains with an average diameter d.[16] The grain boundaries are described by delta-function potentials at which the electron waves can be scattered. The scattering probability is taken into account by the reflection coefficient R. The intrinsic resistivity ρ_i can then be described by

$$\rho_i = \rho_0 \left[1 - \frac{3\alpha}{2} + 3\alpha^2 - 3\alpha^3 \ln\left(1 + \frac{1}{\alpha}\right)\right]^{-1}, \quad (2)$$

with

$$\alpha = \frac{\lambda_e}{d}\frac{R}{1-R}, \quad (3)$$

where ρ_0 is the bulk resistivity and λ_e the electron mean free path (11.8 nm for hexagonal Co)[1]. Hence, ρ_i of the Co films can be described using the two variables d and R. In the simulated curves in Figure 1 (a), d is varied between 4 and 9 nm based on estimations from the TEM images (Figure 2). The reflection coefficient R is adjusted between 0.33 for the highest density films and 0.75 for the lowest density films. Thus, lower film densities can be accounted for by a higher grain-boundary scattering probability.

For low film thicknesses the resistivity increases due to surface scattering. This becomes dominating for films with thicknesses in the range of and below λ_e. The increased resistivity due to surface-scattering ρ_s, can be described according to Sondheimer by[15]

$$\rho_s = \rho_0 \left(1 - \frac{3}{2\kappa}(1-p)\int_0^\infty \left(\frac{1}{t^3} - \frac{1}{t^5}\right)\frac{1-e^{-\kappa t}}{1-pe^{-\kappa t}}\,\mathrm{d}t\right)^{-1}, \quad (4)$$

$$\kappa = \frac{a}{\lambda_e}, \quad (5)$$

with a being the film thickness and p being the specularity parameter. The latter is a phenomenological parameter that accounts for the degree of specular scattering from the interfaces.

To describe the evolution of resistivity with thickness shown in Figure 1, we use the intrinsic resistivity ρ_i from equation (3) as the bulk resistivity ρ_0 in equation (5). The specularity p is set to 0.03 (*i.e.* 97 % diffusive scattering at the surface). While the model describes the resistivity of the HiPIMS -300 V films well, it deviates severely from the experimental data of the other films at low thicknesses. Even setting p to a lower value and thus increasing the resistivity due to surface scattering does not improve the fit. We attribute the deviation to the simplifying assumptions of continuous films in the model. The top-down SEM images of two thinner films in Figure 1 (b-c) show that the 12 nm DCMS -30 V film consists of islands, while the 6 nm HiPIMS -300 V film is still continuous.

To explain the different film morphologies, the different plasma compositions in DCMS and HiPIMS and their influence on the film nucleation and growth have to be considered. In general, thin metal films on oxides grow in the three-dimensional island (Volmer–Weber) mode, due to the large difference in the surface energy of metals (2.522 J/m^2 for Co)[17] and oxides (0.072 J/m^2 for SiO_2)[18]. Continuous metal films on oxides are typically formed only at thicknesses above 10 nm.[19] Ions impinging on the surface, however, can influence the growth mode depending on their energy. [19] Firstly, if the ion energy exceeds the displacement energy of SiO_2, shallow ion implantation of Co can occur.[19,20] Implanted Co is expected to increase the surface energy of SiO_2 and thus decrease the difference in surface energies. Hence, the

density of Co nuclei can be increased substantially. In the HiPIMS discharge, such ions with energies above the displacement energy are always present in the tail of the ion energy distribution function.[11] Secondly, the low energy ions increase the mobility of adsorbed atoms facilitating the growth of larger grains.[21] Lastly, at high ion energy re-sputtering can occur (HiPIMS, -300V), which leads to further densification of the Co films and smoother surfaces. Larger grains can be observed in both HiPIMS and DCMS when comparing the high and low substrate bias. In HiPIMS, however, the fraction of ions is much larger than in DCMS and their effect is hence pronounced already at the low bias voltage.

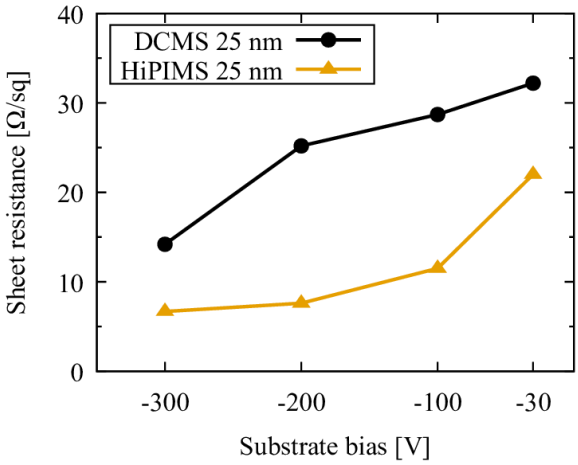

Figure 4 Dependence of the sheet resistance on the substrate bias for Co films with a nominal thickness of 25 nm deposited by DCMS and HiPIMS.

The difference between the Ar^+-ion dominated DCMS plasma with neutral Co atoms and the Co-ion dominated HiPIMS plasma is further illustrated by the dependency of the sheet resistance on the substrate bias shown in Figure 4 for a nominal thickness of 25 nm. In both sputtering configurations, higher ion energies lead to more conductive films. In HiPIMS, however, a bias voltage of -100 V is sufficient to achieve a pronounced reduction in sheet resistance, which is in agreement with results reported for Cu.[14] In DCMS, in contrast, large

reduction occurs only above -200 V. This shows that achieving the same energy per deposited metal atom in DCMS requires much higher bias voltages due to the low ion current.

Moreover, the implantation of Ar into the Co films in DCMS is observed by RBS. About 1.1 % Ar is incorporated into the films sputtered by DCMS at a bias of -300 V, while no Ar is detected in the HiPIMS films. The incorporated Ar may pin the grain boundaries and thereby hinder the grain growth. In addition, Ar incorporation can increase the resistivity of metal films by acting as point defects and thereby electron scattering centers.[22]

Eventually, also the interface roughness is affected by the different growth conditions. Both the Co-SiO_2 interface and the Co surface are much smoother in HiPIMS than in DCMS, see Figure 2. We attribute the smoother Co-SiO_2 interface in HIPIMS to a higher nucleation density resulting from aforementioned reduced surface energy difference due to shallow ion implantation.[23] Furthermore, the high instantaneous flux of Co vapor limits cluster coalescence and thus contributes to the formation of continuous, smooth films.[22] On the contrary, in DCMS the larger difference in surface energies promotes three-dimensional island growth, which leads to rougher interfaces and voids.

In summary, we have explored ionized PVD processes for the deposition of ultrathin Co films suitable for interconnect metallization. In particular, we show depositions on SiO_2 at room temperature that lead to low resistivity of 14 μΩ cm at a thickness of 40 nm and 35 μΩ cm at 6 nm using a HiPIMS process with a bias of -300 V. This is comparable to the best values for Cu where a resistivity of about 20 μΩ cm was reported at a thickness of 7 nm.[24] The high metal ionization in the HiPIMS process leads to shallow ion implantation of Co into SiO_2. Thus, the nucleation density is increased, resulting in smooth interfaces and continuous films at lower thicknesses. The ions also promote surface diffusion and thus formation of larger grains. Furthermore, the ionized process is shown to be beneficial in avoiding Ar

incorporation as well as in reducing the required substrate bias and thus limiting the ion damage to the growing surface. The results are in good agreement with models considering the scattering at grain boundaries as the dominant mechanism for thicker films and surface scattering for very thin films.

The authors would like to thank Oleksandr Bilousov for the XRD measurements. Financial support by the Swedish Foundation for Strategic Research (SSF) via contracts SE13-0033 and RIF14-0053 as well as by the Swedish Research Council via VR-RFI contract C0514401 is acknowledged.

[1] D. Gall, J. Appl. Phys. **119**, 085101 (2016).
[2] M.H. van der Veen, K. Vandersmissen, D. Dictus, S. Demuynck, R. Liu, X. Bin, P. Nalla, A. Lesniewska, L. Hall, K. Croes, L. Zhao, J. Bommels, A. Kolics, and Z. Tokei, in *IITC/MAM* (IEEE, 2015), pp. 25–28.
[3] A.A. Vyas, C. Zhou, and C.Y. Yang, IEEE Trans. Nanotechnol. 1 (2016).
[4] J. Kelly, J.H.C. Chen, H. Huang, C.K. Hu, E. Liniger, R. Patlolla, B. Peethala, P. Adusumilli, H. Shobha, T. Nogami, T. Spooner, E. Huang, D. Edelstein, D. Canaperi, V. Kamineni, F. Mont, and S. Siddiqui, in *IITC/AMC* (IEEE, 2016), pp. 40–42.
[5] M. Wislicenus, R. Liske, L. Gerlich, B. Vasilev, and A. Preusse, Microelectron. Eng. **137**, 11 (2015).
[6] M. Hauschildt, B. Hintze, M. Gall, F. Koschinsky, A. Preusse, T. Bolom, M. Nopper, A. Beyer, O. Aubel, G. Talut, and E. Zschech, Jpn. J. Appl. Phys. **53**, 05GA11 (2014).
[7] J.A. Hamilton, T. Pugh, A.L. Johnson, A.J. Kingsley, and S.P. Richards, Inorg. Chem. **55**, 7141 (2016).
[8] M.M. Kerrigan, J.P. Klesko, and C.H. Winter, Chem. Mater. (2017).
[9] U. Helmersson, M. Lattemann, J. Bohlmark, A.P. Ehiasarian, and J.T. Gudmundsson, Thin Solid Films **513**, 1 (2006).
[10] C.C. Klepper, O.R. Monteiro, E.P. Carlson, and M.D. Keitz, J. Vac. Sci. Technol. B **27**, L14 (2009).
[11] J.T. Gudmundsson, N. Brenning, D. Lundin, and U. Helmersson, J. Vac. Sci. Technol. A **30**, 030801 (2012).
[12] A. Anders, Surf. Coat. Technol. **257**, 308 (2014).
[13] D. Lundin and K. Sarakinos, J. Mater. Res. **27**, 780 (2012).
[14] F. Cemin, D. Lundin, D. Cammilleri, T. Maroutian, P. Lecoeur, and T. Minea, J. Vac. Sci. Technol. A **34**, 051506 (2016).
[15] E.H. Sondheimer, Adv. Phys. **1**, 1 (1952).
[16] A.F. Mayadas and M. Shatzkes, Phys. Rev. B **1**, 1382 (1970).
[17] W.R. Tyson and W.A. Miller, Surf. Sci. **62**, 267 (1977).
[18] E.J. Chibowski, Adv. Colloid Interface Sci. **113**, 121 (2005).
[19] A. Anders, *Cathodic Arcs: From Fractal Spots to Energetic Condensation* (Springer, New York, 2008).
[20] X. Gao, J. Andersson, T. Kubart, T. Nyberg, U. Smith, J. Lu, L. Hultman, A.J. Kellock, Z. Zhang, C. Lavoie, and S.-L. Zhang, Electrochem. Solid-State Lett. **14**, H268 (2011).
[21] F. Cemin, D. Lundin, C. Furgeaud, A. Michel, G. Amiard, T. Minea, and G. Abadias, Sci. Rep. **7**, (2017).
[22] J.M. Warrender and M.J. Aziz, Phys. Rev. B **76**, 045414 (2007).
[23] D. Magnfält, V. Elofsson, G. Abadias, U. Helmersson, and K. Sarakinos, J. Phys. Appl. Phys. **46**, 215303 (2013).
[24] E.V. Barnat, D. Nagakura, P.-I. Wang, and T.-M. Lu, J. Appl. Phys. **91**, 1667 (2002).